Proc. R. Soc. Lond. A **377**, 331–348 (1981)
Printed in Great Britain

An experimental investigation of breaking waves produced by a towed hydrofoil

By J. H. Duncan†
The Johns Hopkins University, Baltimore, Maryland 21218, *U.S.A.*

(*Communicated by M. S. Longuet-Higgins, F.R.S. – Received* 6 *November* 1980)

[Plate 1]

This paper presents the results of experiments on breaking waves produced by towing a submerged, two-dimensional hydrofoil at constant depth and speed. The wave field consists of a breaker followed by a train of lower, non-breaking waves. The breaker has a small zone of turbulent water riding its forward slope; this zone is called the breaking region. Measurements were made of surface height profiles, the vertical distribution of mean horizontal velocity in the wake of the wave, and the vertical thickness of the wake.

The results support the hypothesis that the breaking region imparts a shearing force along the forward slope equal to the component of its weight in that direction. The force produces a turbulent, momentum-deficient wake similar to the wake of a towed, two-dimensional body in an infinite fluid. The vertical thickness of the wake grows in proportion to the square root of distance behind the breaker. The momentum deficit is approximately equal to the maximum momentum flux of a Stokes wave with the same phase speed as the breaker.

The surface profile measurements yield several results: the proper independent variables describing the wave are its speed and the slope of its forward face. The relation between breaking wavelength and speed follows the finite-amplitude Stokes wave equation. The amplitude and the vertical extent of the breaking region are both proportional to the phase speed squared; however, they are not functions of the slope of the forward face of the wave. The breaking region has a small oscillation in its length with a regular period of 4.4 the period of a wave with phase speed equal to the hydrofoil speed. The amplitude of the oscillation diminishes with time. It is believed that this oscillation is due to wave components produced when the foil is started from rest.

1. Introduction

Breaking deep-water surface waves can be categorized as either steady (waves produced by ships or hydrofoils moving at constant speed) or unsteady (whitecaps in a wind–wave system or waves breaking owing to interacting, mechanically generated wavetrains). The two types of waves are similar, however, in that they both include an air-entraining turbulent region riding on the waves' forward face.

† Present address: Hydronautics Incorporated, Laurel, Maryland 20810, U.S.A.

The dynamics of this region are controlled by gravity acting in the down-slope direction and Reynolds stresses acting in the up-slope direction. This paper describes an experimental study of a two-dimensional, steady breaking wave produced by towing a submerged hydrofoil at an angle of attack. The study of this wave, *per se*, is of interest both for practical and scientific reasons. In addition, it is hoped that the knowledge gained will shed some light on the dynamics of unsteady wave-breaking.

Previous studies of breaking waves have generally been concerned with their limiting form before breaking, both for steady waves (Stokes 1847) and unsteady waves (Van Dorn & Pazan 1976; Longuet-Higgins & Cokelet 1976). There have been few investigations of waves that are already breaking. Mason (1951) made qualitative observations of breaker types produced as non-breaking waves approach a beach. A film of shallow-water breaking waves by Kjeldsen & Olsen (1971) was later compared by Longuet-Higgins & Turner (1974) with their theoretical analysis of an unsteady turbulent breaking region growing on the forward face of a wave. By using approximate equations of motion, combined with some related experimental data on air entrainment in free-surface flows, they were able to predict the acceleration of the front of the breaker and some aspects of the shape of the breaking region, both as a function of wave phase speed and the slope of the forward face. Some measurements of the turbulent flow field below whitecaps were reported by Longuet-Higgins (1974*b*) and Donelan (1977). Since the experiments reported here were completed, a similar technique has been used by Battjes & Sakai (1980) to investigate spilling breakers in shallow water.

The breaking waves studied for the present paper were produced by towing a hydrofoil (0.60 m span, 0.20 m chord) horizontally under the water surface at constant speed, depth, and angle of attack in a long towing tank (24 m $\times$ 0.61 m $\times$ 0.61 m). When the foil speed, angle of attack and depth of submergence were adjusted properly, breaking waves of various lengths and slopes were obtained. Photographs of the surface profile and dyed turbulent wake of the breaker appear in figures 1 and 2 (plate 1). A description of the techniques used to obtain these photographs is given later.

Measurements of the surface height profile of the wave field, the vertical distribution of mean horizontal velocity in the wake, and the vertical thickness of the wake were made. The measurement techniques and the experimental apparatus are described in §2. The experimental results are presented in §3. In §4, the data are used to discuss some aspects of the dynamics of the flow. Finally, the conclusions of the work are summarized in §5.

2. Experimental details

2.1. *Apparatus*

Waves were produced by towing a hydrofoil horizontally in a tank that was 24 m long, 61 cm deep, and 61 cm wide (see figure 3). One of the 24 m long side walls of

Proc. R. Soc. Lond. A, volume 377

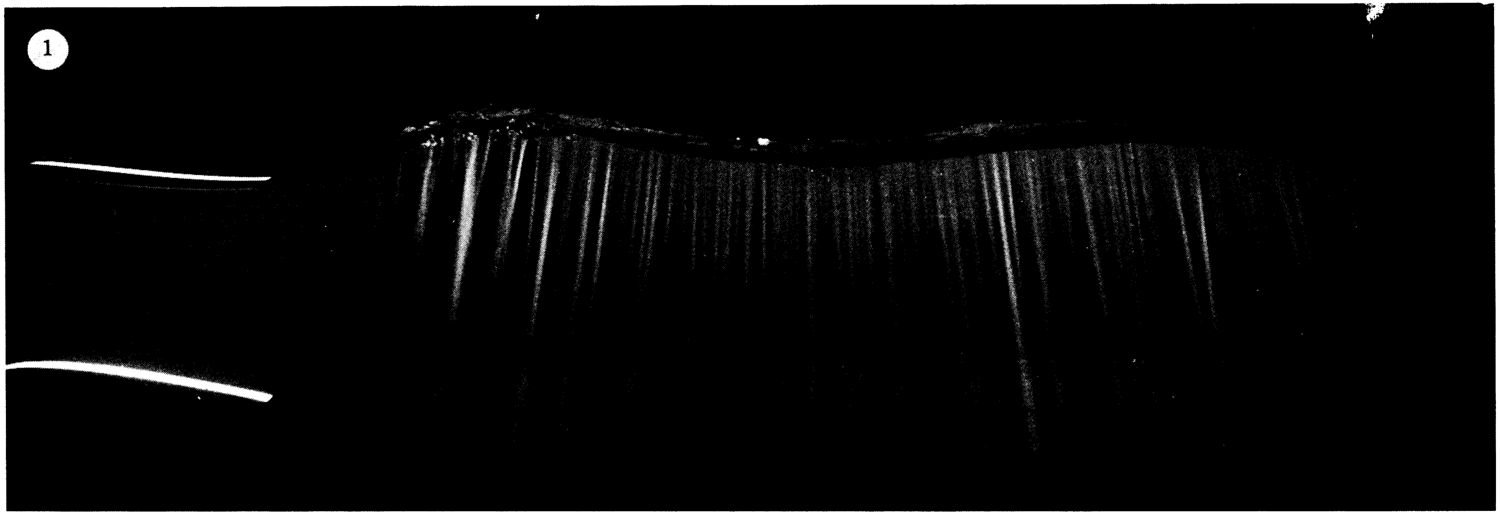

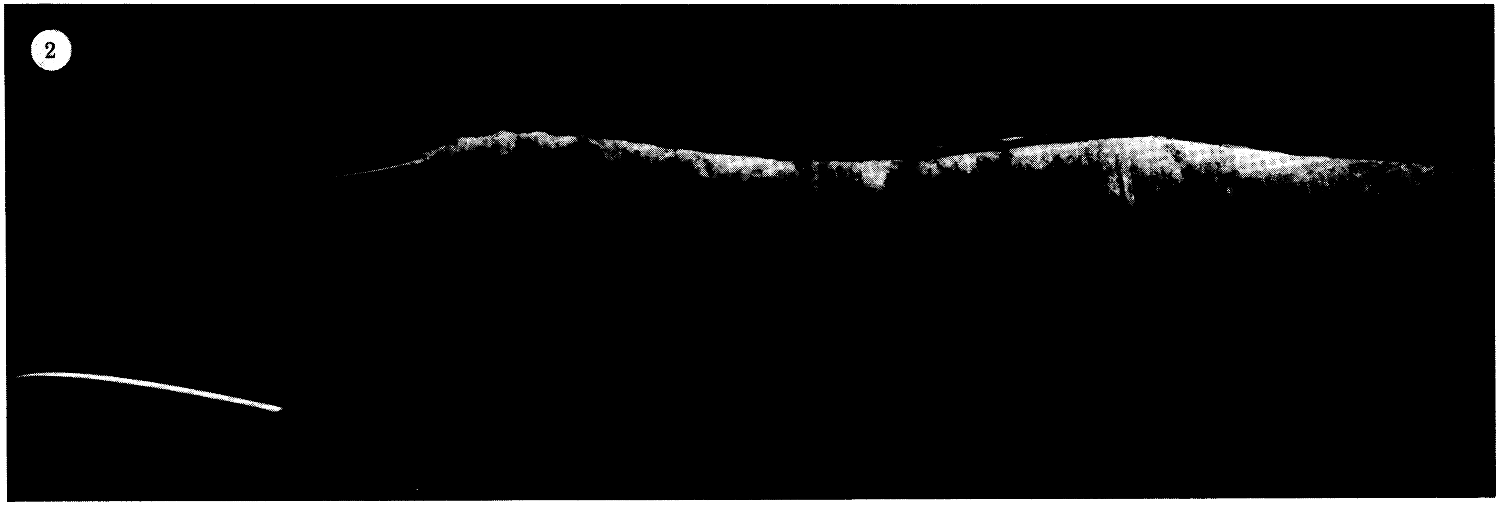

FIGURE 1. A photograph of the surface height profile of a breaking wave. The hydrofoil is in the lower left-hand corner of the picture and is moving from right to left.

FIGURE 2. A photograph of the turbulent wake of a breaking wave. The hydrofoil is in the lower left-hand corner of the picture and is moving from right to left.

(Facing p. 332)

the tank was made of clear Plexiglas, while the other three walls and the bottom were plywood. For photography, the bottom and the 24 m long plywood wall were covered with black cloth. There were ± 0.5 cm variations in the depth and width of the tank.

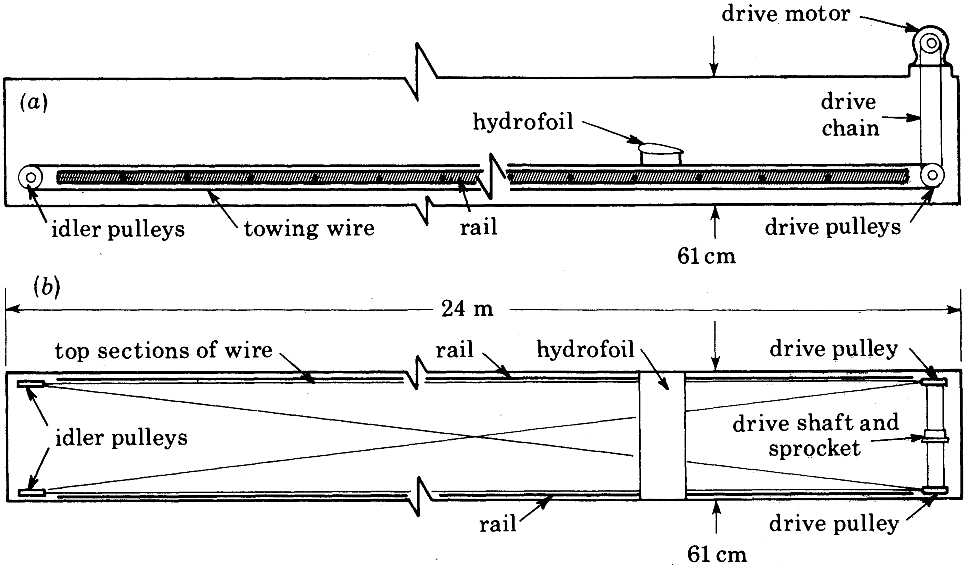

FIGURE 3. Towing tank with hydrofoil and its towing system: (*a*) side view; (*b*) top view.

The hydrofoil had a NACA 0012 shape and was made of solid aluminium. It had a chord of 20.3 cm and a maximum thickness of 2.54 cm at 6.1 cm from the nose. The span of the foil was only 60.0 cm to ensure clearance along the entire tank. There was initial concern that the gaps between the foil edges and the walls, which varied from 2 to 5 mm, might cause unwanted three-dimensional effects. Wave measurements, however, showed no discernible lack of two-dimensionality. The foil was towed along a pair of 20 m long aluminium tracks – one attached to each side of the tank at a nominal distance of 15 cm from the tank bottom. When the installation of the rails was complete, measurements showed that the depth of the rails from the water surface did not vary by more than 0.2 cm at any point in the tank. The foil was attached to the rails via two thin nylon blocks which were bolted to the bottom of the foil on either side. The foil could be set at either a 5 or 10° angle of attack, nose up.

The force for moving the foil through the water was supplied by a wire and pulley towing system (see figure 3). The power for the towing system came from an electric motor and a variable-speed transmission which were mounted on top of the tank. A roller chain and sprocket transmitted power from the motor to the pulley drive shaft. To prevent grease from the roller chain from producing a surface slick on the water, a barrier was placed at the surface next to the chain. The foil could be towed at speeds up to 1.2 m/s with nothing piercing the water surface in the vicinity of the foil. Reproducibility checks on the speed, which were made by timing the foil over 13 m, showed only a 1 % fluctuation in speed at 1.2 m/s.

Surface elevation profiles, wave velocity distributions and wake thicknesses were measured by using either a still or a ciné camera attached to an independently controlled carriage that travelled on top of the tank. The camera was mounted on the carriage by a wooden frame which placed it at a horizontal distance of 1.1 m from the Plexiglas side wall and at various heights. Along with the camera, the carriage contained a light-slit generator consisting of five 500 W photo-floodlights and two vertical metal plates. This device could project a 3 cm thick vertical sheet of light, 1.2 m long, parallel to the long side walls of the tank along the tank's centre. The carriage and hydrofoil were controlled independently; hence the camera and light source could either move with the foil or remain stationary.

2.2. *Measurements*

The surface height profiles were measured photographically by a 16 mm ciné camera with a 10 mm lens. The use of wave height probes was avoided since their operation might have been hindered by air in the breaker. The camera was placed about 15 cm above the water surface and 1.1 m out from the tank side wall, oriented to point slightly down toward the water surface. The water was dyed with $1.5/10^6$ rhodamine WT fluorescent dye. When the lights were on, the vertical sheet of light excited only the dye within the sheet, causing it to fluoresce. The camera then recorded a glowing line on the water surface which, when the wave was present, produced an image of the surface profile at the centre of the tank. A sample photograph appears in figure 1 (plate 1). Distances were measured to an accuracy of about ± 0.2 cm. The average values of the variables describing the breaking region were obtained from films taken in wave-fixed coordinates. The films were analysed by measuring the breaking-region oscillation period for each set of conditions (see §3), and then averaging twelve successive data points taken at time intervals of $\frac{1}{12}$ of the period (each data point was obtained from a single ciné frame). The first measurement was always taken when the foil was at least 6 m from the starting position to ensure a quasi-steady state.

The displacement of near neutrally buoyant particles over a short time interval yielded the vertical distribution of mean horizontal velocity. This rather tedious technique was chosen to avoid the possibility of air bubbles fouling a Pitot tube or hot film probe. With a laser velocimetry system moving with the wave, optical alignment problems would have been experienced. The particles used were polystyrene spheres with an average diameter of 0.5 mm. The specific gravity of the particles was 1.035, which indicates (with the use of a Stokes-law drag force) a sinking rate of 0.5 cm/s. The mean speed of the wave and camera relative to the polystyrene beads was greater than 60 cm/s, so sinking only introduced a small error in the measurements. Estimates of the velocity difference between the particle and the oscillating flow were made. The calculated errors were, at most, 5 % of the velocity fluctuations induced by the following wavetrain.

A Nikon F2 35 mm camera was attached to the instrument carriage moving at the same speed as the wave. The camera was placed 1.1 m to the side of the tank and about 10 cm below the water surface. The camera shutter was left open long enough for a streak to be produced on the film for each illuminated particle; thus the streak length was proportional to the particle speed. Tests were run without the foil to compare the measured particle velocity with the known carriage speed. Variations in the streak lengths between calibration runs were caused by a combination of camera shutter speed variations, camera vibrations, residual motions of the water, carriage speed variations, and inaccuracies in the reading of the films. Even with all these error sources, the standard deviations for the calibration runs in each case were never more than ± 2 % of the mean. This was deemed sufficiently accurate to measure the momentum deficit in the wake of the breaker, since here the velocity was 10–15 % less than the wave phase speed.

The wake was dyed and its evolution filmed to obtain the time history of its vertical thickness. First, a solution of 30 parts water (from the tank) and one part rhodamine WT fluorescent dye was sprayed on the surface, a layer of dye about 0.03 cm thick and 4 m long being created in the centre of the tank. Then the ciné camera was placed at the tank centre, 1.1 m from the side wall, and at the same height as the water surface. After the wave had passed, the dye diffused downward owing to the turbulence. The light source, described previously, illuminated the dye within the slit, causing it to fluoresce. The fluorescence was photographed by the camera, which was set on *f*-1.4 and 24 frames/s with Kodak 4-X reversal black and white film. A sample photograph appears in figure 2 (plate 1). Four to six separate runs were performed for each test condition to get enough realizations for averaging. To obtain the wake's vertical thickness from the films, tracings were made from images projected by a stop-frame projector. The wake edge, which had a very irregular profile, was then smoothed by drawing a line that had approximately equal areas of dye below and undyed water above it.

2.3. *Experimental conditions and procedures*

For all the measurements, the procedure for producing the breaking wave was the same. The water level was set, the surface was skimmed, and the foil was placed 3.2 ± 0.1 m from the end of the tank. A period of at least 20 min was allowed between tests to assure that all visible motions from previous tests had died away. Finally, the driving motor was turned on and, after a short acceleration period, the foil moved along the tank at constant speed.

The experimental conditions given in table 1 were chosen to obtain a reasonable range for the independent variables describing the wave (its phase speed, C, and the angle of inclination of the wave's forward face, θ). The wave speed always equalled the foil speed, but the value of θ could not be determined *a priori*. Seven wave speeds from 62.5 to 103 cm/s were chosen which, according to first-order linear wave theory, correspond to a range of wavelengths from 24 to 68 cm. At five of the speeds, two combinations of water depth and angle of attack were chosen to obtain two values of θ for the same value of C. All of the twelve sets of experimental conditions were used for the surface profile measurements, but only three were used for the wake velocity measurements. The decision to use a small number of test conditions for the wake width and velocity measurements was based on the similarity of the surface profile results and the tedium of making the measurements. Note from table 1 that the foil depth ranged from 0.75 to 1.21 hydrofoil chords, l, and that the Froude number, C^2/gl, varied from 0.19 to 0.53.

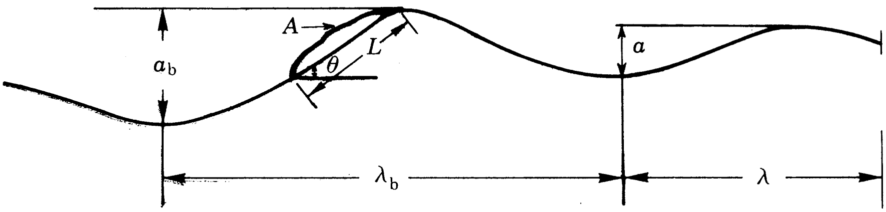

FIGURE 4. Definition sketch for the surface profile variables.

3. Experimental results

The amplitude, a_b, and length, λ_b, of the breaking wave; the length, L, area, A, period of oscillation, T_{br}, and angle of inclination of the breaking region, θ; and the length and amplitude of the following wave train were measured from the surface profile data for each of the twelve sets of experimental conditions. The values of all these measured variables appear in table 1, and a definition sketch appears in figure 4 to aid the reader. In the figure and the data analysis, the bottom of the breaking region that determines L, θ, and A was taken as the tangent to the smooth water surface in front of the breaker.

The first thing to notice from the data is the amount of variation of θ. Table 1 shows a range of θ from 10 to 14.7°. With a standard deviation of about 1.5° at each reading, this indicates that a small, but measurable, change in θ was obtained. Also note that significant changes in θ were obtained while keeping the speed constant. The question of whether or not the ranges in θ and C were large enough to show significant effects in the other dependent variables will be answered by the subsequent presentation. The question of whether or not a larger range of θ could be obtained by other experimental conditions or with another hydrofoil can only be answered by additional experiments.

Figure 5 is a plot of the length of the breaking wave against the phase speed of the wave, C. In addition to the data, the curve $C = 1.044(g\lambda/2\pi)^{\frac{1}{2}}$ for finite-amplitude Stokes waves is plotted. This curve was taken from the theoretical work of Longuet-Higgins (1974a). The slope of the wave which is needed as input to the theory was taken as $\frac{1}{2}a_b g/C^2$, which, by the measurements presented in the following paragraph, always equals 0.3. The figure shows that there is certainly a one-to-one

TABLE 1. EXPERIMENTAL CONDITIONS AND RESULTS

foil speed, C / cm/s	62.5	68.9	70.4	75.0	75.9	81.1	82.0	91.1	91.7	97.5	102.1	103.0
foil angle of attack, α/deg	5	5	10	10	5	10	5	5	10	10	5	10
water depth to chord centre, d/cm	15.3	15.3	20.3	20.3	18.5	20.3	18.5	18.5	24.6	24.6	18.5	24.6
water depth to bottom, D/cm	32.4	32.4	39.1	39.1	35.6	39.1	35.6	35.6	43.3	43.3	35.6	43.3
d/l (l = chord length)	0.75	0.75	1.00	1.00	0.91	1.00	0.91	0.91	1.21	1.21	0.91	1.21
C^2/gl	0.19	0.24	0.25	0.28	0.28	0.33	0.34	0.42	0.41	0.48	0.52	0.53
angle of inclination of breaking region, θ/deg	13.3	11.6	10.0	10.9	14.7	11.0	13.1	13.1	13.9	13.0	13.8	12.7
length of breaking region, L/cm	6.5	7.1	9.7	11.2	7.3	14.5	10.8	14.4	12.3	16.0	16.7	20.5
area of breaking region, A/cm^2	4.6	5.4	9.5	12.4	6.0	20.5	12.6	20.3	16.4	28.9	31.7	39.3
amplitude of breaking wave, a_b/cm	2.4	3.1	3.1	3.4	3.4	3.8	3.9	4.9	5.0	5.2	6.2	6.6
length of breaking wave, λ_b/cm	22.4	30.0	31.6	32.6	33.8	36.3	37.6	47.0	46.3	51.4	60.2	61.9
amplitude of following waves, a/cm	1.0	0.8	1.7	1.2	1.8	1.4	1.9	1.9	2.6	2.6		1.9
length of following waves, λ/cm	22.1	26.5	29.4	33.6	33.6	40.6	40.3	47.1	49.7	58.3		60.3
T_{br}/T_w	5.2	4.3		4.2	no osc.	4.3	3.9	4.4	4.3	4.5	4.6	4.6
wake velocity measurements	yes	no	no	no	yes	no	no	yes	no	no	no	no
wake width measurements	yes	no	no	no	no	yes	no	no	yes	no	yes	no

correspondence between the wavelength and phase speed of the waves and that the data follow the nonlinear wave relation very well. It seems surprising that the phase speed of this asymmetric breaking wave should be nearly equal to that of a symmetric non-breaking wave with the same wavelength.

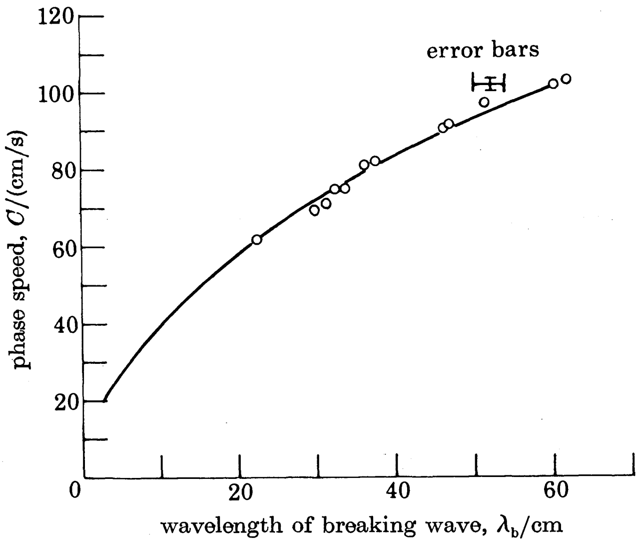

FIGURE 5. Breaking-wave phase speed against wavelength. The curve is from nonlinear Stokes wave theory with slope $\frac{1}{2}a_b g/C^2$.

The amplitudes of the breaking waves – the vertical distance between the trough in front of the breaker and the crest (which is not the same as the vertical distance from the crest to the trough after the breaker) – are shown in figure 6 plotted against C^2/g. The straight line in the figure was fitted to the data and constrained to go through the origin of the graph. This line:

$$a_b = 0.6C^2/g, \tag{1}$$

is a good fit to the data and can be used to relate the amplitude to the phase speed (or wavelength as was shown in the previous paragraph). The five equal-phase-speed pairs of points in the graph were examined for a systematic effect of θ but none could be found. From the data presented so far, the amplitude and wavelength of the breaking waves are functions of C only. Since both λ_b and a_b are proportional to C^2/g, we have $a_b/\lambda_b \approx 0.1$ for all conditions. The reader is cautioned that this is an asymmetric wave; thus the vertical distance from the crest to the trough after the breaker, and the horizontal distance from the first trough to the wave crest, can change while a_b/λ_b remains the same.

To begin the examination of changes in the wave shape while a_b/λ_b is constant, consider some properties of the breaking region. Figure 7 is a plot of the wave amplitude, a_b, against $L \sin\theta$, which is the vertical component of the length of the breaking region. Note that the straight line fitted to these data is a fairly accurate representation, indicating the equation

$$a_b = 1.6L\sin\theta. \tag{2}$$

There is, however, a systematic variation of θ in the five pairs of equal-phase-speed points; the points on the left always have a larger angle. A graph of $a_b/L\sin\theta$ against θ was plotted but no clear trend appeared.

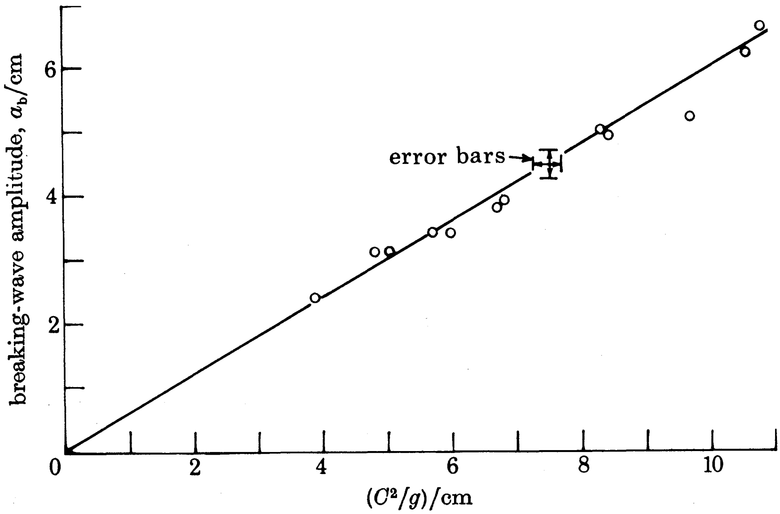

FIGURE 6. Breaking-wave amplitude against C^2/g.

The last parameter of interest describing the breaking wave profile is the average thickness of the breaking region divided by its length (the aspect ratio). This is equal to the area divided by the length squared. By dimensional analysis A/L^2 should be a function of g, θ, and C (surface tension being ignored), but, since the dimensions of g and C cannot be cancelled, one concludes that it is a function of θ only. The data show no trends larger than the standard deviations of the measurement. The average A/L^2 value is 0.11 ± 0.01.

In addition to the steady-state character of the breaking wave, it was noted that the length of the breaking region oscillated during the experimental runs. Measurements of the oscillation period were made by analysis of the ciné films taken in wave-fixed coordinates. The breaking region underwent several cycles during each run, with the number of cycles depending on the speed of the wave. Analysis of the data showed no measurable systematic changes in the period during any experimental run. In fact, even the first period, which includes the breaking of the wave, was the same as the following periods. Qualitative observations showed that the amplitude of the oscillation decreased as the wave progressed and that, in one case, where the wave changed gradually from non-breaking to breaking, there was no oscillation at all. A single-averaged-oscillation period was measured from each run. No trends in the data were discernible, and it was found that the oscillation period was 4.4 ± 0.3 times the period of a linear wave with the same phase speed as the breaking wave.

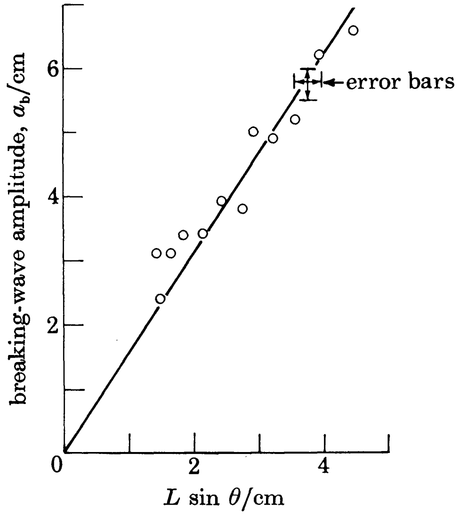

FIGURE 7. Breaking-wave amplitude against the vertical component of the breaking-region length.

Distributions of horizontal velocity against depth, at the first crest after the breaking wave, were measured by the methods described in §2.2 for the three test conditions ($C = 62.5, 75.9, 91.1$ cm/s) marked in table 1. The results of the measurements for $C = 75.9$ cm/s appear in figure 8, which is a plot of the speed against depth. The plot contains the actual data points from the measurements of the particle speeds, points that are averages of the individual data points over 0.5 cm depth intervals, and a curve of the velocity distribution from linear theory for a wave with the same speed and amplitude as the following wave train. Note from the figure that at large depths the linear wave theory and the data points coincide. In the top few centimetres of water, however, the measured velocity is less than the linear theory with the maximum difference of about 20 % of the speed occurring at the surface. A comparison of the data from the three foil speeds shows that both the maximum velocity difference and the depth of the momentum-deficient layer increase with the wave speed.

The time history of the average wake width was measured in a frame fixed relative to the undisturbed water (see §2.2). Data were taken at four of the twelve sets of experimental conditions: $C = 62.5$, 81.1, 91.7, 102.1 cm/s (see table 1). At each condition from three to six experimental runs were performed. The data in each of the four sets were combined by averaging the values at particular times during the runs. The averaged data appear in figure 9, which is a plot of wake

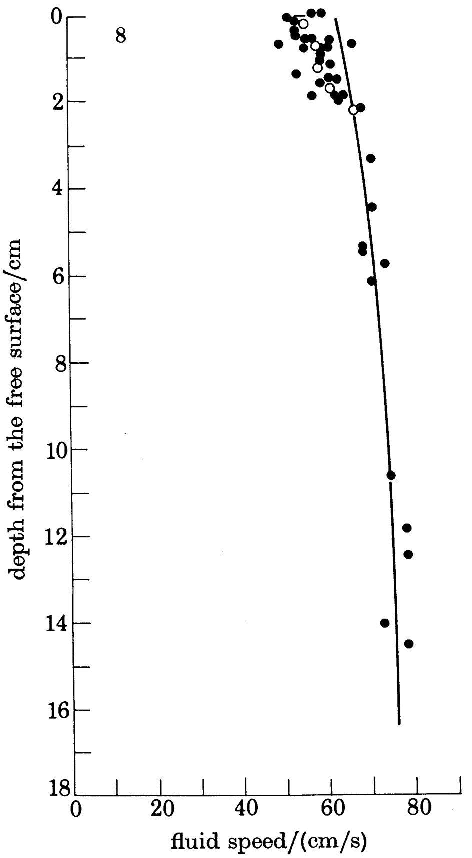

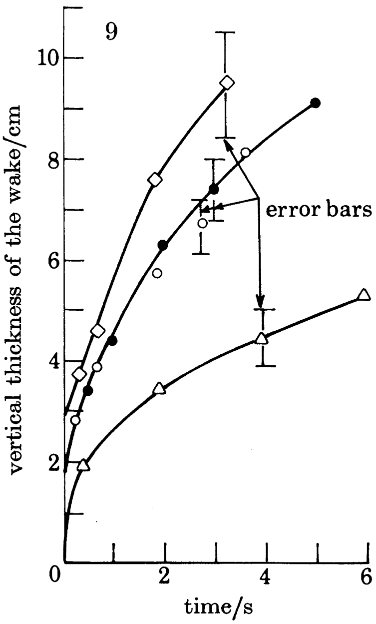

FIGURE 8. Velocity distribution at the crest of the first wave after the breaking wave; foil speed = 75.9 cm/s, angle of attack = 5°; foil depth = 18.5 cm. ●, Data points; ○, averages of data points; the solid curve is from linear Stokes wave theory.

FIGURE 9. Average vertical thickness of the wake against time. △, foil speed = 62.5 cm/s, foil angle of attack = 10°, foil depth = 15.3 cm; ●, 81.1 cm/s, 10°, 20.3 cm; ○, 91.7 cm/s, 10°, 24.6 cm; ◇, 102.1 cm/s, 5°, 18.5 cm.

thickness against time and contains a single curve for each condition. Note the large variability in the wake-growth curves.

4. DISCUSSION

A brief analysis of the wave and its wake will facilitate interpretation of the experimental results. The breaking region can be analysed by writing the vertical and horizontal components of the momentum equation integrated over the breaking region. The bottom boundary of the region is the continuation of the surface streamline (see figure 10). Since it has only a slight curvature, this boundary will be taken as a straight line inclined to the horizontal by an angle θ. The spatially integrated, time-averaged momentum equations are

$$-\int_0^L P\sin\theta\,\mathrm{d}l = \int_0^L \tau\cos\theta\,\mathrm{d}l \quad \text{(horizontal)}, \tag{3}$$

$$\int_0^L P\cos\theta\,\mathrm{d}l = \int_0^L \tau\sin\theta\,\mathrm{d}l - \iint_A \rho' g\,\mathrm{d}a \quad \text{(vertical)}, \tag{4}$$

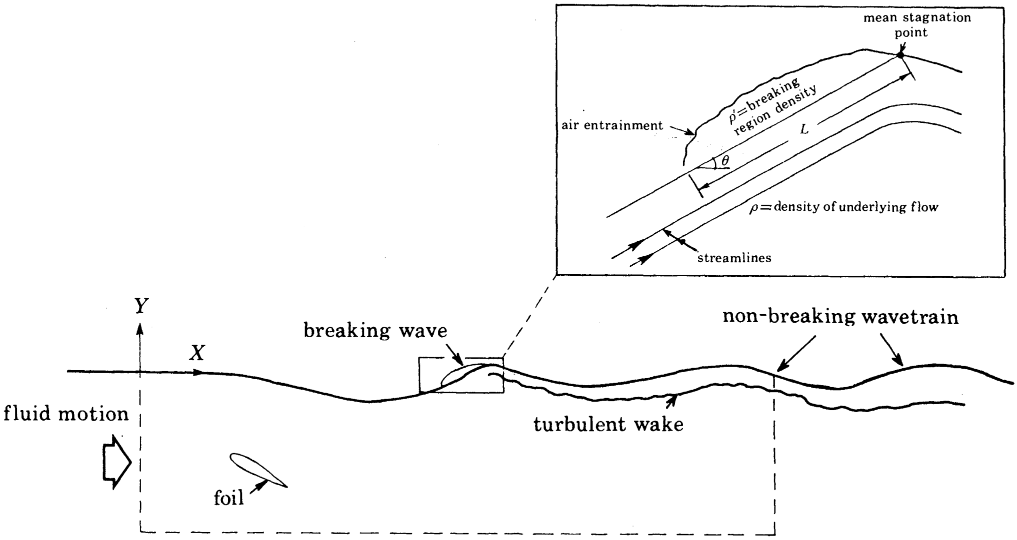

FIGURE 10. Schematic of quasisteady breaking wave and following wavetrain.

where P is the pressure, τ is the Reynolds stress acting tangentially to the bottom boundary of the region, L and $\mathrm{d}l$ are the length and differential length element of the bottom boundary, respectively, ρ' is the density of the breaking region, A and $\mathrm{d}a$ are the area and differential area element of the region, and g is gravitational acceleration. When spatially averaged quantities, denoted by an overbar, are defined, equations (3) and (4) become

$$-\overline{P}\sin\theta\, L = \overline{\tau}\cos\theta L, \tag{5}$$

$$\overline{P}\cos\theta L = \overline{\tau}\sin\theta L - \overline{\rho'} g A. \tag{6}$$

Combining equations (5) and (6), we have

$$\overline{\rho'} g A \sin\theta = \overline{\tau} L. \tag{7}$$

This shows that the tangential component of the weight of the breaking region is balanced by the Reynolds stress acting from below.

To relate the breaking-region dynamics to the wake properties, we now write a spatially integrated horizontal momentum balance over the entire hydrofoil–wave system. This will lead to a formula for the drag on the foil due to the wave breaking.

The dashed line in figure 10 indicates the area over which the momentum equation is integrated. This equation is then

$$\frac{F}{\rho}=\frac{F_{\mathrm{w}}+F_{\mathrm{b}}}{\rho}=\int_{-D}^{\eta}\left(u_1^2+\frac{P_1}{\rho}\right)\mathrm{d}y-\int_{-D}^{\eta}\left(u_2^2+\frac{P_2}{\rho}\right)\mathrm{d}y+\int_{x_1}^{x_2}uv|_{y=-D}\,\mathrm{d}x, \tag{8}$$

where the subscripts 1 and 2 refer to the upstream and downstream ends of the box, respectively, x and y are the horizontal and vertical cartesian coordinates, u and v are the horizontal and vertical velocity components, η is the height of the free surface and ρ is the density. The drag force, F, is divided into two parts – F_{b} due to the wave breaking and F_{w} due to the drag of the small-amplitude wavetrain following the breaker. For the purpose at hand, the drag represented by the wake of the hydrofoil is ignored. To separate the breaking and non-breaking wave drag on the right-hand side of equation (8), it is necessary to define a fictitious downstream state denoted by a subscript w. This new flow field is that of a linear wave with the same amplitude and wavelength as the following wavetrain. (This analysis was first given by Tulin (1951) and later by Wu (1962).) Thus, $u_{\mathrm{w}} > u_2$ inside the turbulent wake and $u_{\mathrm{w}} = u_2$ outside the wake. The drag on the system due to the change in flow from the 1-state to the w-state is then equal to the wave drag, F_{w}, on the hydrofoil plus the negative drag, F_{s}, of the source which is put in the flow to fill in the difference between the velocity profiles u_2 and u_{w}. Thus, we have

$$\frac{F_{\mathrm{w}}+F_{\mathrm{s}}}{\rho}=\int_{-D}^{\eta}\left(u_1^2+\frac{P_1}{\rho}\right)\mathrm{d}y-\int_{-D}^{\eta}\left(u_{\mathrm{w}}^2+\frac{P_{\mathrm{w}}}{\rho}\right)\mathrm{d}y+\int_{x_1}^{x_2}uv|_{y=-D}\,\mathrm{d}y. \tag{9}$$

However, it is known that the thrust of the source can be written

$$\frac{F_{\mathrm{s}}}{\rho}=-C\int_{-\infty}^{\eta}(u_{\mathrm{w}}-u_2)\,\mathrm{d}y, \tag{10}$$

where C is the undisturbed, upstream fluid speed. Combining equations (8), (9) and (10), we obtain the formula for the breaking-wave drag as

$$\frac{F_{\mathrm{b}}}{\rho}=\int_{-\infty}^{\eta}(u_{\mathrm{w}}^2-u_2^2)\,\mathrm{d}y+\int_{-\infty}^{\eta}(P_{\mathrm{w}}-P_2)\,\mathrm{d}y-C\int_{-\infty}^{\eta}(u_{\mathrm{w}}-u_2)\,\mathrm{d}y. \tag{11}$$

Since the streamlines for the w-state and 2-state nearly coincide, $P_{\mathrm{w}} \approx P_2$, and the second term on the right is negligible. Furthermore, since both $u_{\mathrm{w}}-u_2$ and $u_{\mathrm{w}}-C$ are small, equation (11) becomes

$$\frac{F_{\mathrm{b}}}{\rho}=C\int_{-\infty}^{\eta_2}(u_{\mathrm{w}}-u_2)\,\mathrm{d}y. \tag{12}$$

The integral should have the same value anywhere downstream. For the interested reader, a boundary-layer analysis is given in Duncan (1978) which shows that the integral indeed is constant. The non-breaking wave drag is obtained by subtracting equations (10) from equation (9). Using the linear analysis found in Lamb (1945, §248), we have

$$F_{\mathrm{w}} = \tfrac{1}{4}ga^2, \tag{13}$$

where a is the amplitude of the following, non-breaking wavetrain.

It is now possible to hypothesize a relation between the momentum deficit of the wake and the geometry of the breaking region. This will be done by equating the work done by the shear stress at the lower boundary of the breaking region to the

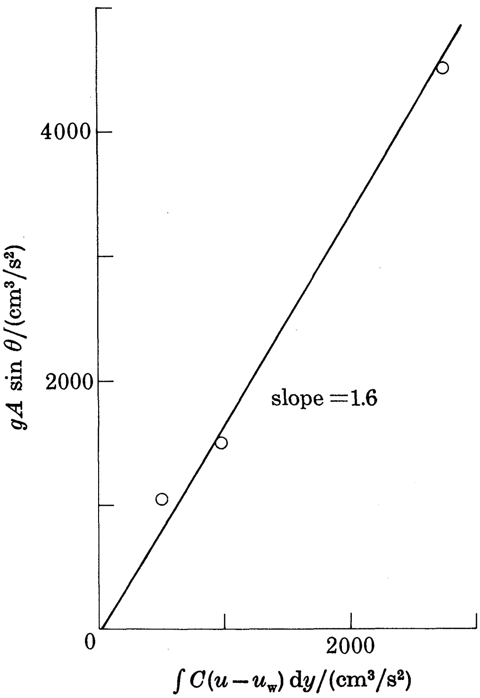

FIGURE 11. Tangential component of the weight of the breaking region against the wake momentum deficit.

energy lost by the mean flow. The work done or energy dissipated by the breaking region is then the drag multiplied by the fluid speed in that region of the flow. We take the speed to be proportional to C, the phase speed of the wave, and the drag to be the average shear stress multiplied by the length of the breaking region, $\bar{\tau}L$. The energy lost by the mean flow must equal the momentum deficit in the wake due to breaking multiplied by the mean flow speed, $F_{\mathrm{b}}C$. When equations (7) and (12) are used in equating the above two energy dissipation rates, one obtains

$$\rho' gA \sin\theta = \rho C \int_{-\infty}^{\eta} (u_2 - u_{\mathrm{w}})\,\mathrm{d}y. \tag{14}$$

The measurements support the above concept of the dynamics of the breaking wave. Equation (7) shows that the force on the flow is proportional to $gA \sin\theta$ (ρ' being ignored for now), and from the surface profile data (equations (1) and (2)), we have

$$gA \sin\theta = 0.015C^4/g \sin\theta. \tag{15}$$

Thus, since waves of the same speed can exist with different θ, they can have different shearing forces on the flow due to the breaking region.

The momentum balance given in equation (14) can be further explored by using the vertical distributions of horizontal mean velocity that were measured in the wake. These velocity profiles (a sample is shown in figure 8) were taken at three sets of conditions (see table 1). The data are summarized in figure 11, in which the integrated momentum deficit (see equation (12)), is plotted against $gA \sin\theta$. The latter, if multiplied by ρ', is the tangential component of the weight of the breaking region. The three data points fall fairly well onto the straight line that is drawn to include the origin of the graph. From the data we have

$$\int_{-\infty}^{\eta} C(u_2 - u_\mathrm{w})\,\mathrm{d}y = 0.61 gA \sin\theta. \tag{16}$$

This would agree with the theoretical equation (14) if ρ'/ρ were 0.61. No ρ'/ρ measurements were taken, but Longuet-Higgins (1974*b*) quoted the probable range of ρ'/ρ as 0.8 to 1.0. In view of the uncertainty in A, then, the theory and experiment are in reasonable agreement. Combining equation (16) with equation (15), we have

$$F_\mathrm{b} = \int_{-\infty}^{\eta} C(u_2 - u_\mathrm{w})\,\mathrm{d}y = \frac{0.009C^4}{g \sin\theta}. \tag{17}$$

A reference drag is needed to assess the magnitude of the drag associated with wave breaking. The most logical one is the momentum flux in a Stokes wave with the same speed as the breaker. The only ambiguity here comes from the need to choose an amplitude for this reference wave. It was decided to use the wave amplitude that produces the maximum momentum flux for a non-breaking wave. Longuet-Higgins (1974*a*) showed that the momentum flux is equal to $4T - 3V$, where T and V are the kinetic and potential energy densities tabulated in his paper. The momentum flux, F_m, reaches a maximum at a slope of $ak = 0.433$; for this slope we have $F_\mathrm{m} = 0.050\rho C^4/g$ or, with the use of equation (17),

$$F_\mathrm{b}/F_\mathrm{m} = 0.18/\sin\theta. \tag{18}$$

For the range of θ in the experiments, $F_\mathrm{b}/F_\mathrm{w}$ varies from 1.03 to 0.71. Thus, the momentum deficit due to wave breaking is about the same as the momentum flux in a limiting-form Stokes wave with the same phase speed as the breaker.

The data on the wake's vertical thickness can also be analysed within the framework of a momentum-deficient wake. Thus it is assumed that, like the wake of a towed body in an infinite fluid, the wake thickness, W, will be a function of time, t, phase speed, C, and the momentum deficit of the wake, $C^4/g \sin\theta$ (see equation (17)).

Using dimensional analysis, we obtain

$$Wg\sin\theta/C^2 = f(tg\sin\theta/C). \tag{19}$$

The data of figure 9 are now plotted in figure 12, in the above non-dimensional form. As can be seen from figure 12, the data collapsed along a single curve. If the wake behaves like a momentum-deficient wake, one would expect the vertical thickness to increase in proportion to the square root of the distance behind the wave. A least-squares-regression analysis was used to fit this power law to the data in the figure. Note that the curve fits the data adequately. The plotted equation is

$$Wg\sin\theta/C^2 = 0.07\,(tg\sin\theta/C - 0.5)^{\frac{1}{2}}. \tag{20}$$

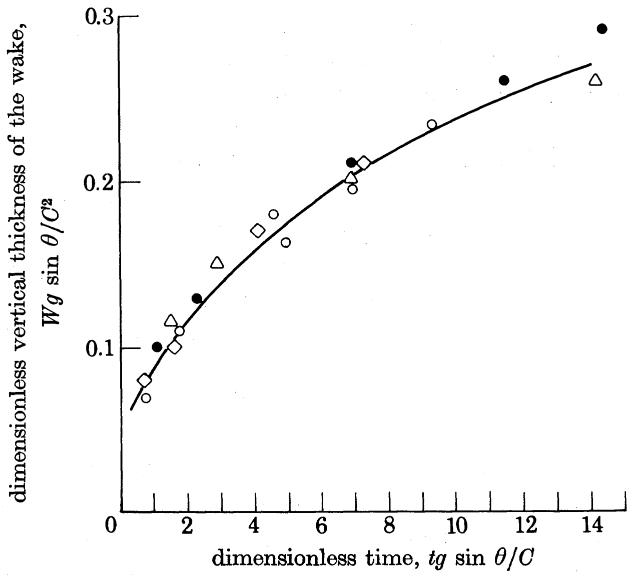

FIGURE 12. Dimensionless vertical thickness of the wake against dimensionless time. Solid line shows $W \propto (C^3/g\sin\theta)^{\frac{1}{2}}t^{\frac{1}{2}}$. See figure 9 for plotting-symbol key.

The above result can be compared with the measurements of the growth of the wake of a towed body in an infinite fluid. First, equation (20) must be recast in terms of the drag on the flow per unit crest length, F_b. Accordingly, equation (20) can be rewritten as

$$W = 0.74(F_b t/\rho C)^{\frac{1}{2}}, \tag{21}$$

the virtual origin being ignored. The result for the width of the wake of a two-dimensional towed body in an infinite fluid is of the same form and has a numerical constant of 0.57 (Schlichting 1968, p. 693) when half the drag and half the wake width are used in the equation.

The surface profile measurements yield several interesting results in addition to supporting the above analysis. The most important is that the independent variables describing the wave are its phase speed and the angle of inclination of its forward face. The wavelength, trough-to-crest amplitude and vertical extent of the breaking region, $L \sin\theta$, are all proportional to the phase-speed squared, C^2, and are independent of the slope of the forward face, θ. All the waves have breaking regions with the same aspect ratio, A/L^2. There is no obvious physical explanation for these latter results. Some theoretical work on breaking regions has been done by Longuet-Higgins & Turner (1974) who predicted that the thickness of the breaking region increases linearly with distance down the wave face. Thus the rate of increase in the thickness is comparable generally with A/L^2. Their results show that, for a slope of $\theta = 15°$, $A/L^2 = 0.1$, which is in agreement with the present findings.

The remaining measurement is the period of oscillation of the breaking region. This was found to be $4.4 \times$ the period of a linear wave with the same phase speed as the breaker. It is believed that this oscillation is due to wave components generated when the foil is started from rest. Let σ_t and k_t denote the frequency and wavenumber of the following wavetrain. Let σ_f and k_f denote similar quantities for the wave component whose group velocity equals the final hydrofoil speed, C. Then, by linear wave theory,

$$\sigma_t = 2\sigma_f \quad \text{and} \quad k_t = 4k_f. \tag{22}$$

If primes denote quantities measured in the frame of the foil, we have

$$\sigma'_f = \sigma_f - Ck_f. \tag{23}$$

Using linear wave theory and equation (22), we can reduce this to

$$\sigma'_f = \tfrac{1}{4}\sigma_t. \tag{24}$$

Thus the period of this wave is 4.0 the period of the steady following waves as compared with 4.4 for the breaking-region oscillation. This is in fairly close agreement.

5. Conclusion

The measurements showed that the breaking region produced a shearing force along the forward face of the wave. The force was equal to the component of the region's weight in the direction of the stress. As a result, a turbulent wake was left behind with a momentum deficit equal to the shearing force. Wake momentum deficit values about equal to the maximum momentum flux of a Stokes wave with the same speed as the breaker were measured. The vertical thickness of the wake was found to increase in proportion to the square root of the distance behind the wave.

A remarkable degree of similarity was found in the geometry of the waves. The wavelength, the crest-to-trough amplitude and the vertical extent of the breaking region were all proportional to the phase-speed squared. Waves with the same phase speed did, however, have various forward-face slopes accompanied by other changes in the wave geometry. The breaking-region thickness divided by its length was found to be the same for all conditions.

This work was supported by the Office of Naval Research (contract no. N00014-76-C-01840), which we gratefully acknowledge.

It is also a pleasure to acknowledge Dr Owen M. Phillips for numerous helpful discussions during the course of this work, and the management of Hydronautics Incorporated for the use of their facilities for the experiments described herein.

REFERENCES

Battjes, J. A. & Sakai, T. 1980 Abstract from *17th Int. Conf. on Coastal Engineering*, Sydney, Australia, March 1980, pp. 370–371. Institution of Engineers, Australia.

Donelan, M. A. 1977 Whitecaps and momentum transfer. *Turbulent fluxes through the sea surface, wave dynamics and prediction* (ed. A. Favre & K. Hasselmann), pp. 273–287. New York: Plenum Press.

Duncan, J. H. 1978 The dynamics of breaking surface waves. Doctoral dissertation, The Johns Hopkins University, Baltimore, Maryland.

Kjeldsen, S. P. & Olsen, G. B. 1971 Breaking waves (16 mm film). Technical University of Denmark, Lyngby.

Lamb, H. 1945 *Hydrodynamics*. New York: Dover Publications.

Longuet-Higgins, M. S. 1974*a* Integral properties of periodic gravity waves of finite amplitude. *Proc. R. Soc. Lond.* A **342**, 157–175.

Longuet-Higgins, M. S. 1974*b* Breaking waves – in deep or shallow water. *Proc. 10th Symposium on Naval Hydrodynamics, Cambridge, Mass.*, pp. 597–605. Arlington, Virginia: Office of Naval Research.

Longuet-Higgins, M. S. & Cokelet, E. D. 1976 The deformation of steep surface waves. *Proc. R. Soc. Lond.* A **350**, 1–26.

Longuet-Higgins, M. S. & Turner, J. S. 1974 An 'entraining plume' model of a spilling breaker. *J. Fluid Mech.* **63**, 1–20.

Mason, M. A. 1951 Some observations of breaking waves. In *Gravity waves*. National Bureau of Standards Circular 521.

Schlichting, H. 1968 *Boundary-layer theory*. New York: McGraw-Hill.

Stokes, G. G. 1847 On the theory of oscillatory waves. *Trans. Camb. phil. Soc.* **8**, 441.

Tulin, M. P. 1951 The separation of viscous drag and wave drag by means of the wake survey. David Taylor model basin report 772.

Van Dorn, W. G. & Pazan, S. E. 1976 Laboratory investigations of wave breaking. Scripps Institution of Oceanography, ref. no. 75-21.

Wu, J. 1962 The separation of viscous from wave making drag of ship forms. *J. Ship Res.* **4**, 23–39.